JOURNAL OF MATERIALS SCIENCE 21 (1986) 3581–3589

Determination of the activation energies for nucleation and growth of crystal nuclei in metallic glasses

Q. C. WU*, M. HARMELIN, J. BIGOT, G. MARTIN
CNRS, Centre d'Etudes de Chimie Métallurgique, 15 rue Georges Urbain, 94407 Vitry-sur-Seine Cedex, France

A mathematical procedure is proposed in order to determine separately the activation energy for nucleation, E_n, and for growth, E_g, from isothermal crystallization experiments on metallic glasses. Differential scanning calorimetry (DSC) is used in the isothermal mode to estimate the crystalline fraction as a function of time. The model deals only with polymorphic and eutectic growth. $Cu_{60}Zr_{40}$ amorphous alloys produced with different quenching rates are taken as an example for demonstrating the ability of the proposed method. It is shown that the number of pre-nuclei can be related to the conditions of the initial quench.

1. Introduction

It is of prime importance to elucidate the fundamentals of nucleation and growth for an understanding of crystallization kinetics of amorphous phases [1–7]. However, though the mathematical description of the theory of nucleation and growth is well developed in the literature [8], the basic problem of determining separately the activation energy for nucleation, E_n, and the activation energy for crystal growth, E_g, remains difficult to solve in a practical way. Nucleation and growth always progress simultaneously during the crystallization process. Nucleation may be homogeneous or heterogeneous, internal or at the surface. Nuclei may be quenched-in or formed during annealing. Growth may be primary, eutectic or polymorphic according to the composition of the amorphous system.

In this paper, an attempt is made to develop a method for extracting E_n and E_g from isothermal crystallization experiments and to compare the number of nuclei in amorphous ribbons quenched from the melt according to different procedures. $Cu_{60}Zr_{40}$ amorphous alloys were chosen to test the proposed method because their crystallization behaviour is of the polymorphic-type and is highly dependent on the quenching conditions [9–15]. Differential scanning calorimetry (DSC) was used in the isothermal mode to determine the crystalline fraction as a function of time.

2. Experimental procedure

The $Cu_{60}Zr_{40}$ master alloy (~ 30 g) was prepared by levitation melting of electrolytic copper and Kroll zirconium under helium. This was then broken into ~ 3 g fragments and these were successively quenched from the melt by planar flow casting. We have here considered three distinct ribbons and these have been prepared under slightly different conditions (see Table I). Each ribbon was ~ 7 mm wide.

As-quenched samples were systematically studied by X-ray diffraction using Co$K\alpha$ radiation and a diffracted-beam graphite monochromator. No traces of Bragg peaks were detected: the results presented here were obtained from fully amorphous specimens.

A Perkin–Elmer DSC-2C device connected to a 3500 thermal analysis data station (TADS) was used for the measurements. The amorphous specimens (typically 3 to 4 mg) were put in an aluminium pan and held in place by a gold cover. The same pan and cover were used for all experiments. The atmosphere was pure argon. The following procedure was chosen in order to reduce the possibility of atomic diffusion leading to the formation of new nuclei: the temperature, T_a, of each isothermal treatment was reached by first heating at a rate of 320 K min^{-1} from ambient temperature up to ($T_a - 10$ K) and then reducing the heating rate sequentially to 20 K min^{-1} up to T_a. When the temperature T_a was reached, the isothermal TADS program was simultaneously started and the rate of enthalpy change against time was automatically recorded by the TADS device until crystallization was completed. The recording rate was chosen in order to obtain a time interval ~ 2.5 sec between two data points. All data were stored on disk and later on processed by a program which was designed taking the following theoretical considerations into account.

3. Theoretical considerations

The kinetics of crystallization of metallic glasses is often described by the well-known phenomenological Johnson–Mehl–Avrami equation:

$$x(t) = 1 - \exp[-K(t - \tau)^m] \quad (1)$$

Permanent address: WU Qin-Chong, Institute of Solid State Physics, Chinese Academy of Sciences, Hefei, China.

0022–2461/86 $03.00 + .12

TABLE I Experimental conditions used to prepare by planar flow casting the amorpous $Cu_{60}Zr_{40}$ ribbons investigated in this work

Ribbon		Initial temperature of the melt (°C)	Argon pressure (mbar)
Symbol	Thickness ($\pm 5\,\mu$m)		
A	30	1300	150
B	35	1150	150
C	40	1150	250

Quenching technique, planar flow casting; atmosphere, helium; crucible, silica; nature of the wheel, copper.

where $x(t)$ is the crystalline fraction at time t, τ the so-called incubation time and m the Avrami exponent*. K is defined as the effective overall reaction rate constant. K and τ are usually assigned Arrhenian temperature dependences:

$$K(T) = K_0 \exp(-mE/RT) \quad (2a)$$

$$\tau(T) = \tau_0 \exp(+E_\tau/RT) \quad (2b)$$

where T is the absolute temperature, R the gas constant, E the activation energy describing the overall crystallization process, and E_τ the activation energy for incubation.

The two kinetic parameters E and m can be obtained from the DSC isothermal experimental data on annealing at different temperatures. However, the values of E and m thus determined are purely phenomenological: m reflects the nucleation rate and/or the growth morphology, E is only an apparent value which cannot represent the respective contributions of nucleation and growth mechanisms.

In the following, a model is proposed which handles separately nucleation and growth and deals only with polymorphic and eutectic growth. The nucleation rate, I, and the crystal growth rate, u, are assumed to have Arrhenian temperature dependences with activation energies E_n and E_g, respectively:

$$I = I_0 \exp(-E_n/RT) \quad (3)$$

$$u = u_0 \exp(-E_g/RT) \quad (4)$$

and the model is cast in such form as to extract E_n and E_g separately.

Two cases are considered.

1. If no pre-existing nuclei are present, the number of crystal nuclei formed per unit volume during the time interval between t and $(t + dt)$ is $I dt$. Assuming a three-dimensional growth of the nuclei, a crystal growth rate independent of the crystal size and of the fraction transformed, the increase in volume during the time interval between t and $(t + dt)$ for a crystal nucleated at t' may be formally written as:

$$4\pi\gamma u^3 [f(t, t')]^2 \, dt \quad (5)$$

where γ is a geometric shape factor (e.g. $\gamma = 1$ for spherical crystal growth).

In the following, we restrict our topic to isothermal annealing. An extension of the model to transient annealing is proposed in the Appendix.

For an isothermal transformation process, the total transformed (crystallized) fraction at t is:

$$x(t) = \int_\tau^t I_0 \exp\left(-\frac{E_n}{RT}\right) dt' \int_{t'}^t 4\pi\gamma u_0^3 \times \exp\left(-\frac{3E_g}{RT}\right) [f(t'', t')]^2 \, dt'' \quad (6)$$

where τ is the time for onset of nucleation and $f(t'', t') = (t'' - t')$.

In order to take into account the overlap of nuclei (for nucleation and crystal growth) during the crystallization process, the statistical overlap function $g(x)$ is introduced and Equation 6 becomes:

$$x(t) = \int_\tau^t I_0 \exp\left(-\frac{E_n}{RT}\right) dt' \int_{t'}^t 4\pi\gamma g(x'') u_0^3 \times \exp\left(-\frac{3E_g}{RT}\right) (t'' - t')^2 \, dt'' \quad (7)$$

where x'' is the transformed fraction at t''.

2. If there are some pre-nuclei in the as-quenched specimen and if their size is assumed to be the same for simplicity:

$$x(t) = \int_\tau^t I_0 \exp\left(-\frac{E_n}{RT}\right) dt' \int_{t'}^t 4\pi\gamma g(x'') u_0^3 \times \exp\left(-\frac{3E_g}{RT}\right) (t'' - t')^2 \, dt'' + N_0 \int_0^t 4\pi\gamma g(x'') u_0^3 \times \exp\left(-\frac{3E_g}{RT}\right) [f(t'', 0)]^2 \, dt'' \quad (8)$$

where N_0 is the number of pre-nuclei and $f(t'', 0) = t''$. Equation 8 may also be written as:

$$x(t) = G \exp\left(-\frac{E_n + 3E_g}{RT}\right) \int_\tau^t dt' \times \int_{t'}^t g(x'')(t'' - t')^2 \, dt'' + \frac{GN_0}{I_0} \times \exp\left(-\frac{3E_g}{RT}\right) \int_0^t g(x'') t''^2 \, dt'' \quad (9)$$

where $G = 4\pi\gamma u_0^3 I_0$.

If Equation 9 is differentiated with respect to t, it becomes: (i) when $t \geqslant \tau$

$$\frac{dx}{dt} = G \exp\left(-\frac{E_n + 3E_g}{RT}\right) g(x) \int_\tau^t (t - t')^2 \, dt' + \frac{GN_0}{I_0} \exp\left(-\frac{3E_g}{RT}\right) g(x) t^2 = g(x) \left[\frac{G}{3} \exp\left(-\frac{E_n + 3E_g}{RT}\right) (t - \tau)^3 + \frac{GN_0}{I_0} \exp\left(-\frac{3E_g}{RT}\right) t^2\right] \quad (10a)$$

(ii) when $0 \leqslant t < \tau$

$$\frac{dx}{dt} = g(x) \frac{GN_0}{I_0} \exp\left(-\frac{3E_g}{RT}\right) t^2 \quad (10b)$$

*In order to avoid any confusion with the symbol "n" used for nucleation m has been chosen in this paper for the Avrami exponent.

Taking the overlap function $g(x) = 1 - x$ as is usually done [16–18], separating variables and integrating, we get:

$$-\ln(1-x) = P(T)(t-\tau)^4 + Q(T)t^3 \quad t \geqslant \tau \tag{11a}$$

and

$$-\ln(1-x) = Q(T)\,t^3 \quad 0 \leqslant t < \tau \tag{11b}$$

or

$$x = 1 - \exp[-P(t-\tau)^4 - Qt^3] \quad t \geqslant \tau \tag{12a}$$

and

$$x = 1 - \exp\{Qt^3\} \quad 0 \leqslant t < \tau \tag{12b}$$

Here:

$$P(T) = (G/12)\exp[-(E_n + 3E_g)/RT] \tag{13a}$$

and

$$Q(T) = (GN_0/3I_0)\exp\{-3E_g/RT\} \tag{13b}$$

Thus, from isothermal transformation experimental data at different temperatures T and using Equations 11a and b and a linear regression method, the values $P(T)$ and $Q(T)$ are obtained. If ln $P(T)$ and ln $Q(T)$ are plotted against $1/T$, N_0/I_0 can be determined.

If there are no pre-nuclei in the as-quenched specimen, then $Q = 0$ in Equation 12a, i.e.:

$$x = 1 - \exp\{-P(t-\tau)^4\} \tag{14}$$

If the nucleation rate equals zero (i.e. saturation of point sites), $P = 0$ in Equation 12a, i.e.:

$$x = 1 - \exp(-Qt^3) \tag{15}$$

Equations 14 and 15 have the Johnson–Mehl–Avrami (JMA) form (Equation 1) but $m = 4$ for Equation 14, and $m = 3$ for Equation 15. These are the two extreme cases.

If the JMA form (Equation 1) is taken to fit the isothermal transformation experimental data, instead of Equation 12a the reaction rate K and the Avrami exponent m are, in some way, mathematical averages of the values for P and Q and of 3 and 4. K and m are mathematical fitting parameters which have meaning only at a given temperature T.

Combining Equations 13a and b, it is possible to define a number γ associated with the number of quenched-in nuclei N_0 in the amorphous specimen and the nucleation rate at a given temperature:

$$\gamma = \ln\left[\frac{4N_0}{I_0\exp(-E_n/RT)}\right] = \ln Q - \ln P \tag{16}$$

4. Results and discussion

Typical DSC traces on heating are shown in Fig. 1. The exothermic and irreversible structural relaxation process (indicated by the difference in the traces q and r [19, 20]) and the temperature range of glass transition were similar for the three ribbons investigated.

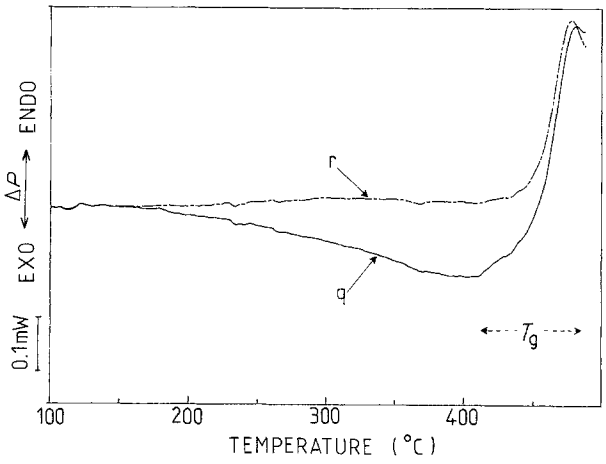

Figure 1 Typical DSC curves on heating $Cu_{60}Zr_{40}$ amorphous samples: curve q, first heating of an as-quenched specimen from ambient temperature up to 490° C; curve r, second heating of the same specimen after having cooled it from 490° C down to room temperature at 320 K min^{-1}. Heating rate for both scans: 80 K min^{-1}. DSC curves are normalized to 1 mg sample weight.

The temperature range of the series of isothermal anneals was chosen within the glass transition interval, as indicated in Fig. 1. Thus, nucleation and crystal growth progressed as each sample was in the metastable equilibrium state of supercooled liquid.

The DSC trace from a typical isothermal anneal of an as-quenched specimen is shown in Fig. 2 (trace q). After an initial transient period (a) lasting about 12 sec, there was a slightly endothermic drift (b) of the trace, before the start of the main exothermic effect (c) which we attribute to crystallization. The steady state of the base line (d) was obtained after crystallization was completed. In order to characterize more precisely the transient period, a second isothermal treatment was performed at the same annealing temperature with the same specimen, after having cooled it in the crystallized state down to room temperature and heated it again under exactly the same conditions as in the first heating of the as-quenched state (Fig. 2, trace r). Then, a supplementary transient exothermic deviation of trace q is revealed.

The incubation time, τ, was tentatively measured as the time elapsed between the start of the isothermal anneal and the beginning of the main exothermic effect, as shown in Fig. 2. This measurement may be considered as valid for two reasons: first, as the time elapsed on heating the as-quenched specimen from room temperature up to the temperature of the anneal is very short (~ 100 sec), nucleation is highly improbable. Second, as the annealing temperature was chosen within the glass transition range, incubation time coincides with the time necessary for the transition from the amorphous state to the supercooled liquid state to be completed.

The fraction transformed, $x(t)$, up to any time, t, was taken as proportional to the fractional area of the main exothermic peak, between time τ up this time t. The extrapolation of the base line above the peak is shown in Fig. 2. The x values against time relationships for each annealing temperature are shown in Fig. 3. They are of the usual sigmoidal type.

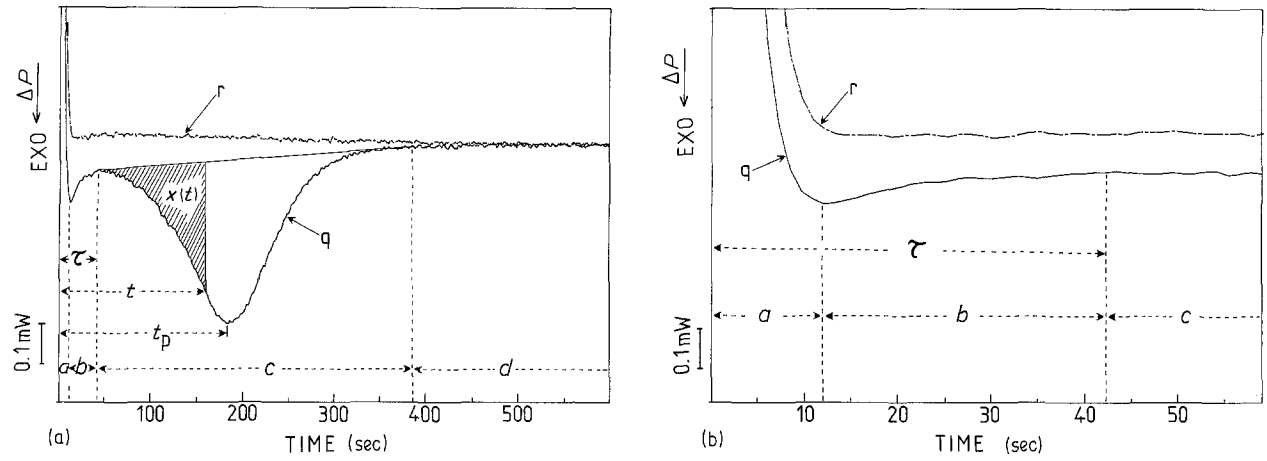

Figure 2 Isothermal DSC curves typical of the $Cu_{60}Zr_{40}$ amorphous alloys. In this experiment, the specimen was cut from ribbon (B), $T_a = 741$ K, $\tau = 42$ sec and $t = 384$ sec for $x = 1$; curve q, first scan of the as-quenched specimen; curve r, second scan after crystallization. DSC curves are normalized to 1 mg sample weight.

Values of the incubation time, τ, coefficients K and m of the JMA Equation 1 and coefficients P and Q of the proposed method (Equations 11a and b) are listed in Table II for each temperature and for each ribbon. Plots of $\ln \tau$, $\ln K$ (from Equation 1), $\ln (t_p - \tau) = E/RT - (1/m) \ln (K_0 m/(m - 1))$ where τ and t_p are defined in Fig. 2, $\ln P$ and $\ln Q$ against $1/T$ are shown in Figs 4 to 8. We can see in Fig. 5 that the scatter of data points for the rate constant K in the Avrami equation is higher than for the coefficients P and Q of the proposed method (Figs 7 and 8).

The corresponding values of the activation energies derived from each plot are indicated in Table III with the coefficients of the linear relationships. As the endothermic drift of part b in Fig. 2 is probably due to glass transition which ends at the time τ, the activation energy derived from the linear relationships $\ln \tau$ against $1/T$ can tentatively be interpreted as the activation energy for viscous flow. The Avrami exponents m for the different ribbons cannot be distinguished one from the other.

The final results are summarized in Table IV. The calculated values of the activation energies for nucleation and for growth are given for the three ribbons with a comparison of the number of quenched-in nuclei and incubation time. These values suggest the following conclusions.

1. The activation energies for nucleation are greatly different for the ribbons A, B and C and the error in this determination is high because E_n is the difference of two values. At the present time, the origin of the differences is not surely established. We think [21] that the evidence for the trend seen in Table IV, i.e. τ is decreasing as v and E_n are increasing, may be understood only in the frame of the heterogeneous nucleation. This trend was clearly confirmed during isothermal crystallization of $Cu_{40}Zr_{60}$ amorphous

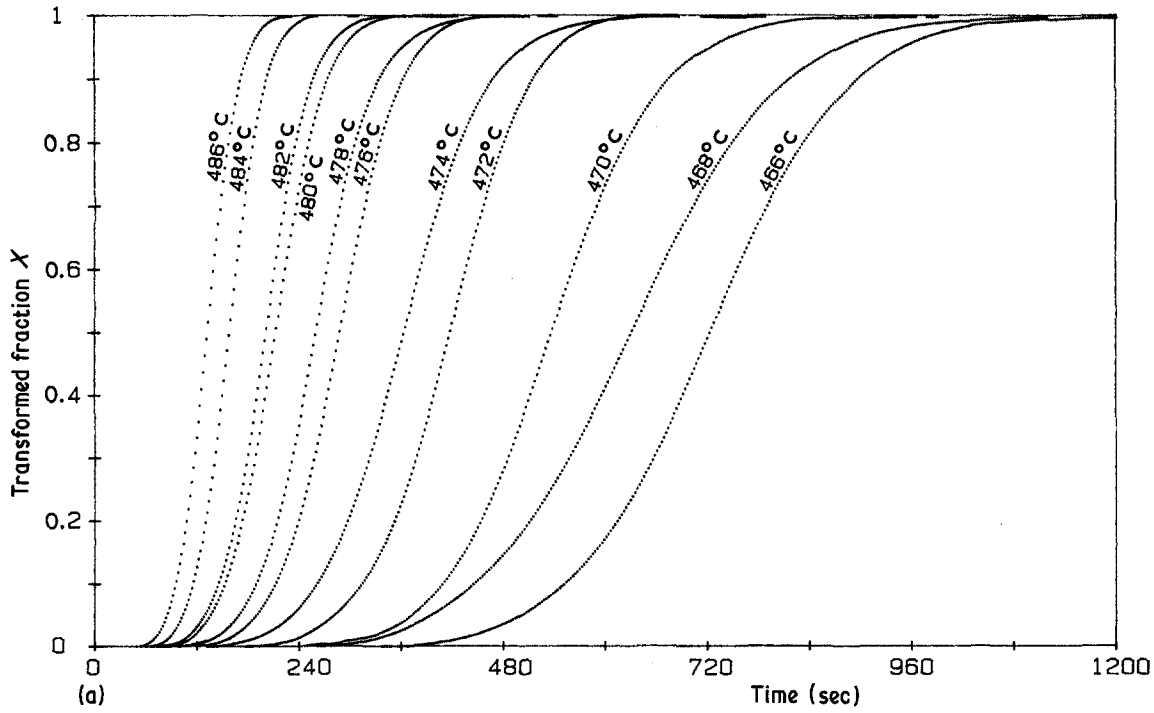

Figure 3 The transformed fraction x against time for ribbons (a) A, (b) B, and (c) C, of $Cu_{60}Zr_{40}$ (T_a in Celsius).

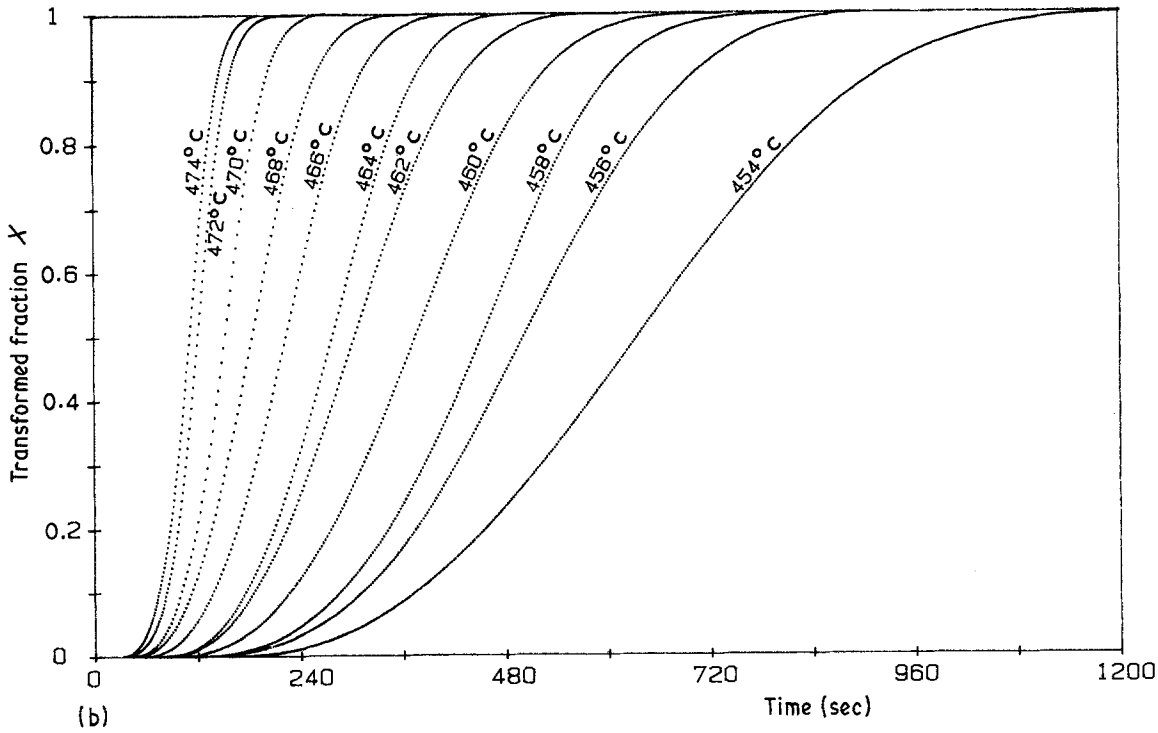

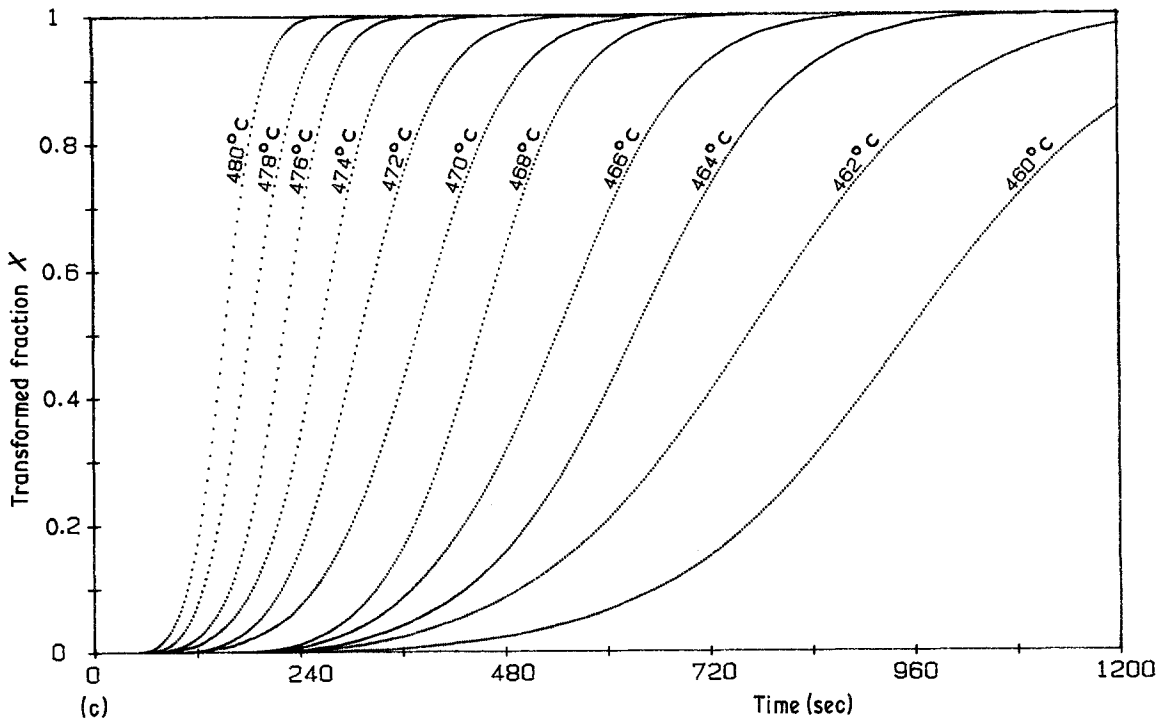

Figure 3 continued.

specimens [22] containing very few quenched-in nuclei.

2. The activation energies for growth appear to be constant for ribbons A, B and C within experimental error: this would be expected.

3. The number of pre-nuclei is smaller in ribbon A than in ribbon B. Consequently, this indicates that there is some advantage in increasing the temperature of the melt prior to the quench. However, this conclusion must be considered with caution because some contamination by the silica crucible is then possible.

4. The number of pre-nuclei is smaller in ribbon C than in ribbon B. Consequently, this indicates that the increase in pressure improves the quality of the quench in the conditions used in this test. The visual confirmation of this was given by the fact that the numbers of bubbles on the wheel-side of the ribbon was smaller than on the external side when the ejection pressure was increased. This corresponds to a higher heat transfer coefficient between the ribbon and the wheel during the quench and thus to a higher quenching rate.

5. The incubation time, greater for ribbon C than for ribbon B, supports this conclusion.

5. Conclusions

In this paper a mathematical procedure is proposed in order to determine separately the activation energies

TABLE II Values of τ, K and m, P and Q for the three $Cu_{60}Zr_{40}$ amorphous ribbons investigated*

Ribbon	T_a (K)	τ (sec)	$-\ln(1-x) = K(t-\tau)^m$			$-\ln(1-x) = P(t-\tau)^4 + Qt^3$		
			K ($\times 10^{-9}$)	m	D ($\times 10^{-2}$)	P ($\times 10^{-12}$)	Q ($\times 10^{-9}$)	D ($\times 10^{-2}$)
A	759	49	668	3.1	3.3	6150	167	5.6
	757	63	372	3.2	2.2	4140	84.7	5.2
	755	76	131	3.2	4.0	1370	43.5	6.2
	754	72	335	3.1	3.0	1870	55.6	5.4
	753	82	221	3.1	2.3	1070	39.5	5.5
	752	95	171	3.0	4.9	678	21.8	4.4
	751	97	40.8	3.3	7.4	441	22.1	7.5
	750	105	85.1	3.1	5.8	461	21.9	7.1
	749	115	28.8	3.3	2.9	453	11.7	5.1
	748	137	37.0	3.2	6.8	210	10.8	7.7
	747	129	13.0	3.3	5.3	110	7.66	6.3
	746	154	29.8	3.1	2.9	135	5.95	5.4
	745	174	4.47	3.4	2.9	143	2.52	3.3
	743	244	8.23	3.2	6.2	45.7	2.24	7.6
	741	256	33.0	2.8	3.3	13.7	1.69	6.0
	739	335	2.79	3.2	2.9	17.7	0.733	5.8
B	748	28	644	3.2	2.8	10900	384	4.1
	747	31	856	3.1	5.6	8570	229	2.5
	746	30	485	3.2	3.0	6690	291	4.2
	745	35	328	3.3	2.6	6000	195	4.3
	744	38	643	3.1	2.7	3140	202	4.6
	743	40	267	3.1	3.7	1970	103	3.0
	742	42	616	2.9	1.6	910	107	2.8
	741	42	883	2.7	3.6	355	86.6	2.1
	740	47	78.5	3.2	6.4	993	39.9	2.2
	739	52	422	2.8	4.4	206	45.5	2.0
	738	60	55.3	3.2	6.1	383	22.3	2.2
	737	71	172	2.9	6.2	146	19.5	1.2
	736	66	45.4	3.1	5.0	147	17.0	2.8
	735	80	655	2.6	4.5	46.1	20.3	1.9
	734	67	48.7	3.0	4.7	59.6	13.4	2.4
	733	87	143	2.7	5.6	25.7	9.76	1.5
	732	100	37.4	2.9	5.4	36.6	6.42	1.6
	731	113	26.0	2.9	8.5	26.1	3.73	0.81
	730	103	129	2.6	5.4	8.98	5.80	1.26
	729	111	25.1	2.9	3.3	8.69	3.84	1.65
	728	123	5.64	3.0	10	8.83	1.40	0.89
	727	153	141	2.5	5.4	1.72	2.33	1.3
C	753	48	154	3.3	3.6	2730	99.2	4.6
	752	51	126	3.3	1.2	1870	67.2	3.3
	751	55	158	3.1	2.6	997	67.0	3.8
	750	68	162	3.1	1.8	885	45.6	4.5
	749	66	10.3	3.6	2.8	829	19.0	3.5
	748	73	10.9	3.5	3.3	648	18.4	4.0
	747	74	9.31	3.5	3.4	361	12.3	3.2
	746	88	9.05	3.4	2.6	296	11.1	3.8
	745	93	14.6	3.3	3.9	140	12.3	4.5
	744	113	109	2.9	2.1	105	12.0	4.4
	743	101	6.30	3.3	2.7	66.9	56.1	3.0
	742	120	3.12	3.4	2.9	63.4	4.00	3.9
	741	153	1.08	3.6	2.4	64.9	1.94	3.1
	740	147	0.356	3.7	1.9	36.2	1.13	2.1
	739	157	1.98	3.3	3.8	20.0	1.64	2.7
	738	157	1.14	3.3	5.3	13.7	1.10	1.9
	737	197	3.53	3.1	4.2	10.4	1.29	3.5
	736	199	0.182	3.5	3.3	7.85	0.432	1.3
	735	206	5.17	3.0	5.1	2.95	0.906	2.9
	733	249	0.144	3.4	3.5	1.48	0.382	4.2

*$D = (\Sigma_{n=1}^{N} d_i^2)^{1/2}/(n-1)$ is the standard deviation of $\ln(1/1-x)$ against t; d_i is the deviation between the experimental point d_i and the fitted curve; T_a is the annealed temperature.

for nucleation and growth for crystallization of a metallic glass. The example of the isothermal crystallization behaviour of $Cu_{60}Zr_{40}$ amorphous ribbons, produced with different quenching conditions, shows that we can distinguish the relative thermal stability of the different ribbons as a function of their respective number of quenched-in nuclei.

The method can be extended to other fields; for instance, the influence of the specimen position along the ribbon (beginning, centre or end of the ribbon),

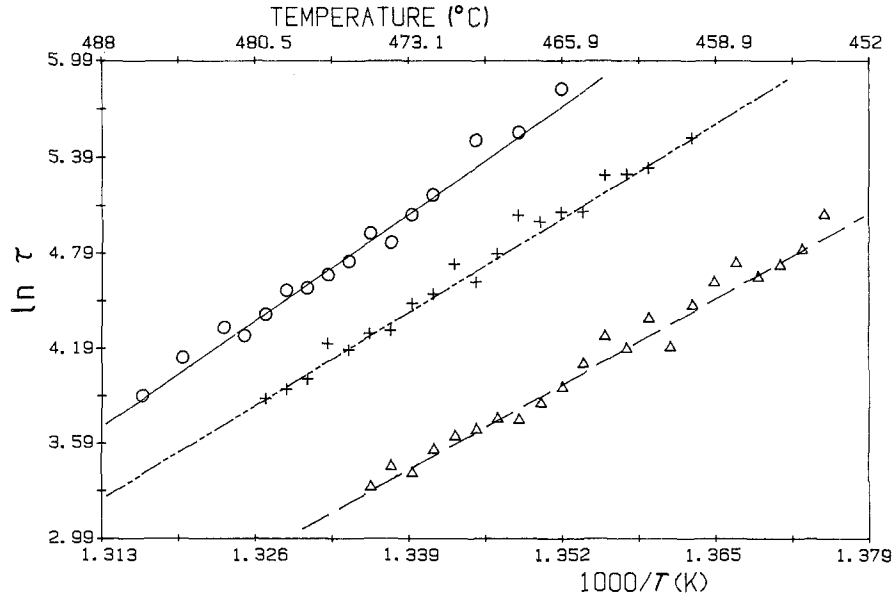

Figure 4 Plots of ln τ against T^{-1} for the (○) A, (△) B and (+) C $Cu_{60}Zr_{40}$ ribbons (τ = incubation time, $T = T_a$ = annealing temperature).

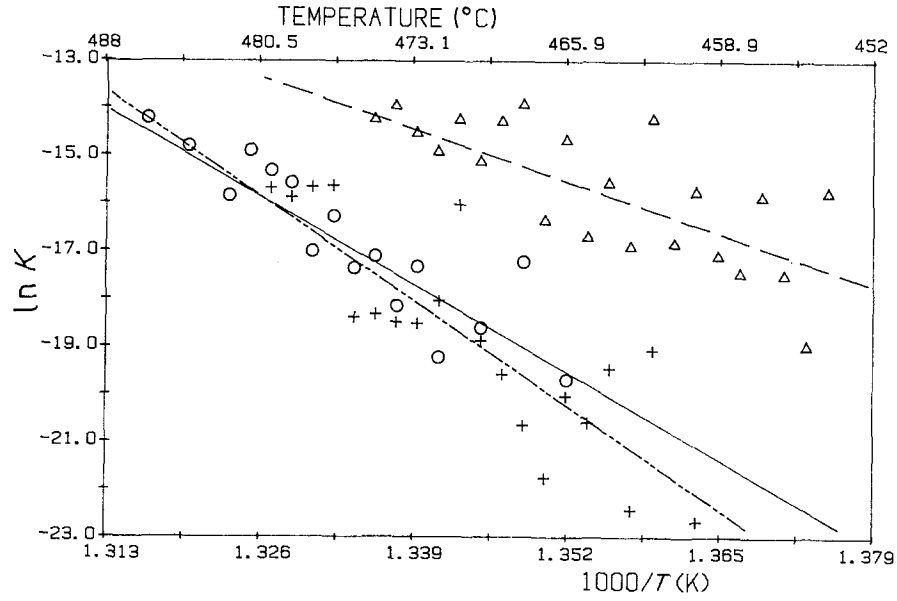

Figure 5 Plots of the overall reaction rate constant, ln K against T^{-1} for the (○) A, (△) B and (+) C $Cu_{60}Zr_{40}$ ribbons ($K = K_0 \exp(-mE/RT)$; $T = T_a$ = annealing temperature).

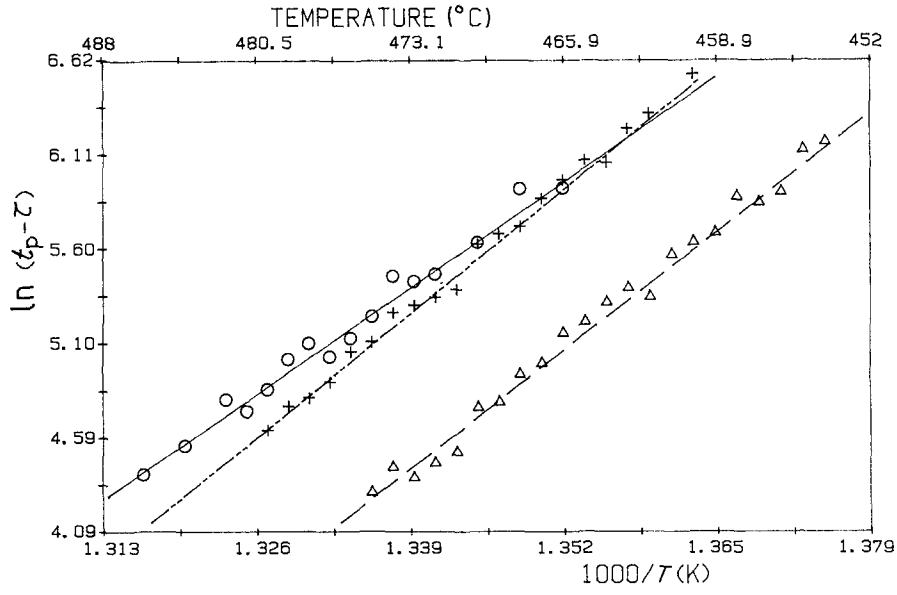

Figure 6 Plots of ln ($t_p - \tau$) against T^{-1} for the (○) A, (△) B and (+) C $Cu_{60}Zr_{40}$ ribbons (t_p and τ as defined in Fig. 2; $T = T_a$ = annealing temperature).

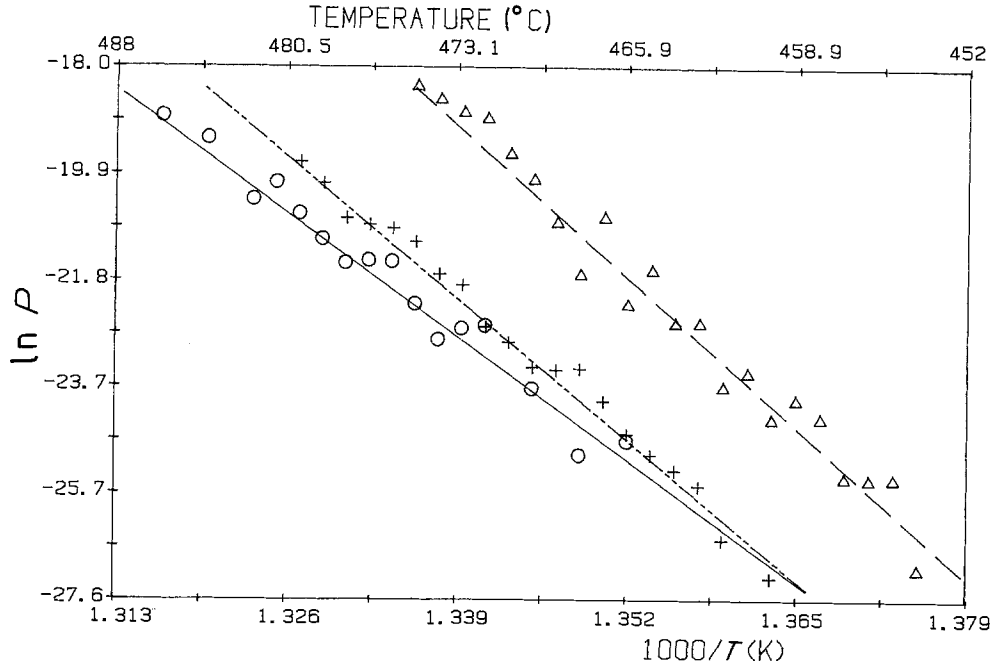

Figure 7 Plots of ln P against T^{-1} for the (○) A, (△) B and (+) C $Cu_{60}Zr_{40}$ ribbons: $P = (G/12)\exp[-E_n + 3E_g)/RT]$; $T = T_a$ = annealing temperature.

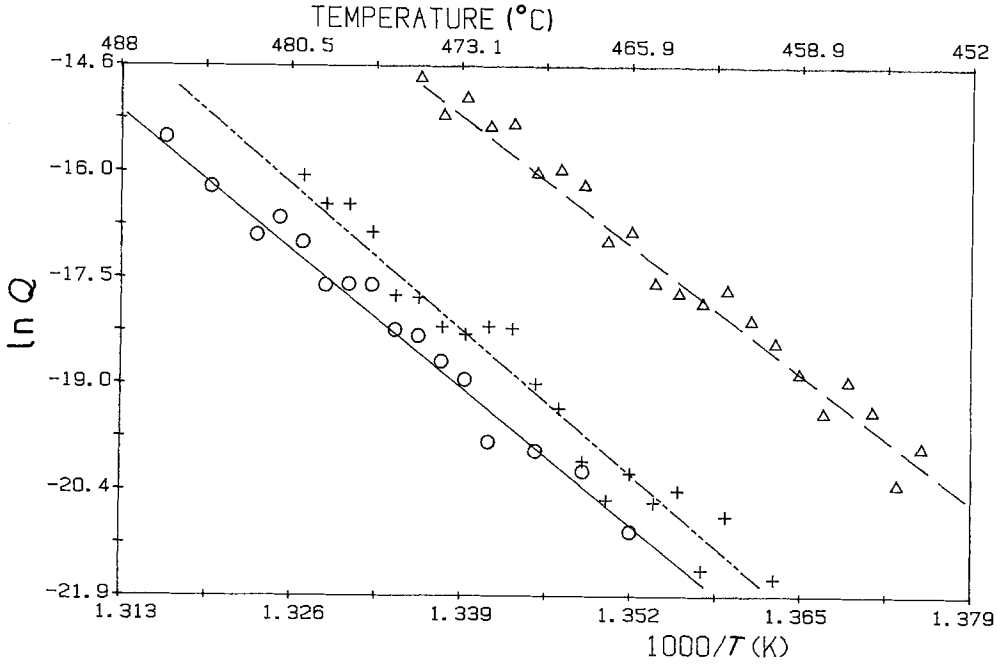

Figure 8 Plots of ln Q against T^{-1} for the (○) A, (△) B and (+) C $Cu_{60}Zr_{40}$ ribbons: $Q = (GN_0/3I_0)\exp(-3E_g/RT)$; $T = T_a$ = annealing temperature.

the effect of the experimental conditions on structural relaxation prior to crystallization and a comparison between alloys with different copper contents.

Acknowledgements

Thanks are due to Y. Calvayrac and J. P. Chevalier for helpful discussions and to A. Quivy for the X-ray diffraction investigations of the amorphous ribbons. Q. C. Wu is very grateful to the Centre National de la Recherche Scientifique of France for a financial grant for his stay at CECM-Vitry.

Appendix

For an anisothermal crystallization process, the function $f(t, t')$ in Equations 6 to 8 must be written as:

$$f(t, t') = \int_{t'}^{t} u(\lambda)\,\mathrm{d}\lambda/u(t) \qquad \text{(A1)}$$

where $u(t)$ is a function of time only because it is a function of temperature (and now temperature is a function of time).

For the same reason, the incubation time now also depends on time. Thus, Equations 6 to 8 are valid only by introducing $H(x)$, the Heaviside function ($H(x) = 0$ if $x < 0$ and $H(x) = 1$ if $x \geqslant 0$) and become, respectively,

$$x(t) = \int_0^t I_0 \exp\left(-\frac{E_n}{RT'}\right) H[t' - \tau(T')]\,\mathrm{d}t' \times \int_{t'}^{t} 4\pi\gamma u_0^3 \exp\left(-\frac{3E_g}{RT''}\right)[f(t'', t')]^2\,\mathrm{d}t'' \qquad \text{(A2)}$$

TABLE IIIa Values of ln τ, ln K and $\bar{m}$ in the JMA equation, ln $(t_P - \tau)$ in the "peak-time" method, ln P and ln Q in the proposed method

	Ribbon A	Ribbon B	Ribbon C
ln τ	$(52.6 \pm 1.7)\,10^3/T - (65.3 \pm 2.3)$	$(42.4 \pm 1.4)\,10^3/T - (53.3 \pm 1.8)$	$(46.1 \pm 1.3)\,10^3/T - (57.3 \pm 1.8)$
ln K	$-(144 \pm 18)\,10^3/T + (175 \pm 24)$	$-(87 \pm 17)\,10^3/T + (102 \pm 23)$	$-(172 \pm 25)\,10^3/T + (212 \pm 34)$
$\bar{m}(\pm 0.2)$	3.2	3.0	3.3
ln $(t_P - \tau)$	$(44.2 \pm 1.6)\,10^3/T - (53.8 \pm 2.1)$	$(49.6 \pm 1.1)\,10^3/T - (62.0 \pm 1.5)$	$(51.8 \pm 0.9)\,10^3/T - (64.1 \pm 1.2)$
ln P	$-(174 \pm 8)\,10^3/T + (210 \pm 10)$	$-(213 \pm 8)\,10^3/T + (266 \pm 10)$	$-(200 \pm 5)\,10^3/T + (245 \pm 7)$
ln Q	$-(149 \pm 5)\,10^3/T + (181 \pm 7)$	$-(139 \pm 5)\,10^3/T + (172 \pm 6)$	$-(157 \pm 7)\,10^3/T + (192 \pm 10)$

TABLE IIIb Comparison of the activation energies (kJ mol^{-1}) derived from these equations

	Ribbon A	Ribbon B	Ribbon C
ln τ	$E = 437 \pm 14$	$E = 353 \pm 12$	$E = 383 \pm 11$
ln K	$E = 374 \pm 50$	$E = 241 \pm 50$	$E = 433 \pm 67$
ln $(t_P - \tau)$	$E = 368 \pm 13$	$E = 412 \pm 9$	$E = 431 \pm 8$
ln P	$\frac{E_n + 3E_g}{4} = 362 \pm 16$	$\frac{E_n + 3E_g}{4} = 443 \pm 16$	$\frac{E_n + 3E_g}{4} = 416 \pm 10$
ln Q	$E_g = 413 \pm 14$	$E_g = 385 \pm 14$	$E_g = 435 \pm 19$

TABLE IV Comparison of E_n, E_g (kJ mol^{-1}), v and ln τ for the three amorphous $Cu_{60}Zr_{40}$ ribbons investigated

	Ribbon A	Ribbon B	Ribbon C
E_n	208 ± 108	615 ± 108	358 ± 100
E_g	413 ± 14	385 ± 14	435 ± 19
v	$25 \times 10^3/T - 29$ $(v)_A$*	$73 \times 10^3/T - 95$ $\approx 2.6(v)_A$	$43 \times 10^3/T - 53$ $\approx 1.6(v)_A$
ln τ	$(\ln \tau)_A$	$\approx 0.79(\ln \tau)_A$	$\approx 0.88(\ln \tau)_A$

*"A" refers to ribbon A. The values of v and ln τ for ribbon A are taken as the unit value.

$$x(t) = \int_0^t I_0 \exp\left(-\frac{E_n}{RT'}\right) H[t' - \tau(T')]\,dt' \times \int_{t'}^t 4\pi\gamma g(x'')u_0^3 \exp\left(-\frac{3E_g}{RT''}\right)[f(t'', t')]^2\,dt'' \quad \text{(A3)}$$

and

$$x(t) = \int_0^t I_0 \exp\left(-\frac{E_n}{RT'}\right) H[t' - \tau(T')]\,dt' \times \int_{t'}^t 4\pi\gamma g(x'')u_0^3 \exp\left(-\frac{3E_g}{RT''}\right)[f(t'', t')]^2\,dt'' + N_0 \int_0^t 4\pi\gamma g(x'')u_0^3 \exp\left(-\frac{3E_g}{RT''}\right)[f(t'', 0)]^2\,dt'' \quad \text{(A4)}$$

where T' and T'' are, respectively, the temperatures at time t' and t''.

References

1. U. KOSTER and U. HEROLD, in "Glassy metals I", edited by H. J. Guntherodt and H. Beck, Topics in Applied Physics, Vol. 46 (Springer Verlag, 1981) p. 225.
2. A. L. GREER, in "Rapidly Quenched Metals", Proceedings of the 5th International Conference, edited by S. Steeb and H. Warlimont, Vol. I (North-Holland, 1985) p. 215.
3. C. V. THOMSON, A. L. GREER and F. SPAEPEN, *Acta Metall.* **31** (1983) 1883.
4. S. RANGANATHAN and M. VON HEIMENDAHL, *J. Mater. Sci.* **16** (1981) 2401.
5. M. G. SCOTT and P. RAMACHANDRARAO, *Mater. Sci. Engng.* **29** (1977) 137.
6. E. G. BABURAJ, G. K. DEY, M. J. PATNI and R. KRISHNAN, *Scripta Metall.* **19** (1985) 305.
7. V. R. V. RAMANAN and G. E. FISH, *J. Appl. Phys.* **53** (1982) 2273.
8. J. W. CHRISTIAN, "The Theory of Transformations in Metals and Alloys" (Pergamon, 1975).
9. Z. ALTOUNIAN, TU GUO-HUA and J. O. STROM-OLSEN, *J. Appl. Phys.* **53** (1982) 4755.
10. K. H. J. BUSCHOW, *J. Appl. Phys.* **52** (1981) 3319.
11. *Idem, J. Phys. F: Met. Phys.* **14** (1984) 593.
12. Y. CALVAYRAC, M. HARMELIN, A. QUIVY, J. P. CHEVALIER and J. BIGOT, *J. Phys. Suppl. 8* **41** (1980) C8-114.
13. M. HARMELIN, Y. CALVAYRAC, A. QUIVY, J. P. CHEVALIER and J. BIGOT, *Scripta Metall.* **16** (1982) 703.
14. J. P. CHEVALIER, Y. CALVAYRAC, A. QUIVY, M. HARMELIN and J. BIGOT, *Acta Metall.* **31** (1983) 465.
15. M. LASOCKA and M. HARMELIN, *Scripta Metall.* **18** (1984) 1091.
16. T. J. W. DE BRUIJN, W. A. DE JONG and P. J. VAN DEN BERG, *Thermochim. Acta* **45** (1981) 315.
17. T. KEMENY and L. GRANASY, *J. Non-Cryst. Solids* **68** (1984) 193.
18. K. MATUSITA, T. KOMATSU and R. YOKOTA, *J. Mater. Sci.* **19** (1984) 291.
19. M. HARMELIN, Y. CALVAYRAC, A. QUIVY, J. BIGOT, P. BURNIER and M. FAYARD, *J. Non-Cryst. Solids* **61/62** (1984) 931.
20. M. HARMELIN, A. SADOC, A. NAUDON, A. QUIVY and Y. CALVAYRAC, *ibid.* **74** (1985) 107.
21. G. MARTIN, in "Solid State Phase Transformations in Metals and Alloys" (Les Editions de Physique, Orsay, 1978) p. 337.
22. Q. C. WU, M. HARMELIN, Y. CALVAYRAC and J. BIGOT, unpublished results.

Received 18 July
and accepted 18 December 1985